# ON THE GRADIENT LINE OF THE MOON'S ZONAL GRAVITATIONAL POTENTIAL FIELD

WALTER KÖHNLEIN

*Institut für Astrophysik und Extraterrestrische Forschung, University of Bonn, Germany*

(Received 10 January, 1973)

**Abstract.** The analytical expression of the gradient line, i.e. the perpendicular to the Moon's zonal equipotential surfaces is derived. Being a sensitive indicator of the geometric structure of the gravitational field, the shape of the trajectory, its direction field and curvature, the points of inflection, etc., are computed at elevations 0 km, 250 km, 1000 km and 10000 km above the Moon's surface. The numerical results were derived from the coefficients of Liu and Laing (1971) and are compared – whenever suitable – with the results obtained from the coefficients of Michael *et al.* (1969).

## 1. Equation of the Trajectory

The zonal gravitational potential $U$ of the Moon can be described by

$$U = \frac{GM}{r}\left[1 - \sum_{n=2}^{\infty}\left(\frac{a}{r}\right)^n J_n P_n(\sin\phi)\right], \tag{1}$$

where $GM$ is the gravitational constant $\times$ mass of the Moon, $a$ is the mean equatorial radius, $P_n$ is the $n$th degree Legendre's polynomial, $J_n$ is the corresponding harmonic coefficient, and $r$ is the selenographic distance to a point in the selenographic latitude $\phi$. Equation (1) is valid in the case of

$$\operatorname{div}\operatorname{grad} U = 0, \tag{2}$$

i.e., in empty space where Laplace's equation is satisfied.

The gradient line is everywhere perpendicular onto the potential surfaces $U = \text{const}$ and satisfies identically the differential equation

$$\frac{\mathrm{d}\mathbf{x}}{\mathrm{d}s} + \frac{\operatorname{grad} U}{|\operatorname{grad} U|} = 0, \tag{3}$$

wherein $\mathbf{x}$ is the position vector referred to the mass center of the Moon, and $s$ is the arc length of the trajectory. To integrate (3), we switch to the polar coordinate system $r$, $\phi$ in which case the differential equation can be written

$$\begin{bmatrix} -\dfrac{\dfrac{\partial U}{\partial r}}{\operatorname{grad} U} & \dfrac{\dfrac{\partial U}{\partial \phi}}{r\operatorname{grad} U} \\ -\dfrac{\dfrac{\partial U}{\partial \phi}}{r\operatorname{grad} U} & -\dfrac{\dfrac{\partial U}{\partial r}}{\operatorname{grad} U} \end{bmatrix} \begin{bmatrix} \cos\phi \\ \sin\phi \end{bmatrix} = \begin{bmatrix} \dfrac{\mathrm{d}x^1}{\mathrm{d}s} \\ \dfrac{\mathrm{d}x^3}{\mathrm{d}s} \end{bmatrix} \tag{4}$$

*The Moon* **6** (1973) 384–397. *All Rights Reserved*

or

$$\begin{bmatrix} \dfrac{\mathrm{d}r}{\mathrm{d}s} & -r\dfrac{\mathrm{d}\phi}{\mathrm{d}s} \\ r\dfrac{\mathrm{d}\phi}{\mathrm{d}s} & \dfrac{\mathrm{d}r}{\mathrm{d}s} \end{bmatrix} \begin{bmatrix} \cos\phi \\ \\ \sin\phi \end{bmatrix} = \begin{bmatrix} \dfrac{\mathrm{d}x^1}{\mathrm{d}s} \\ \dfrac{\mathrm{d}x^3}{\mathrm{d}s} \end{bmatrix}. \tag{5}$$

If we compare the elements in the above left hand matrices, Equation (3) transforms to

$$\frac{\mathrm{d}r}{\mathrm{d}s} + \frac{1}{|\mathrm{grad}\, U|}\frac{\partial U}{\partial r} = 0, \tag{6}$$

$$\frac{\mathrm{d}\phi}{\mathrm{d}s} + \frac{1}{r^2\, |\mathrm{grad}\, U|}\frac{\partial U}{\partial \phi} = 0, \tag{7}$$

in which the arc length $s$ appears only implicitly. Hence a simplified version

$$\frac{\mathrm{d}r}{\mathrm{d}\phi} = r^2 \frac{\partial U}{\partial r}\bigg/\frac{\partial U}{\partial \phi} \tag{8}$$

obtains, which can be integrated with the help of the differential equations (Hobson, 1955)

$$\begin{gathered} \frac{\mathrm{d}}{\mathrm{d}\phi} P_n(\sin\phi) - \frac{1}{\cos\phi}(n+1)\left[\sin\phi\, P_n(\sin\phi) - P_{n+1}(\sin\phi)\right] = 0, \\ (n+1)\, P_n(\sin\phi) + \mathrm{tg}\,\phi \frac{\mathrm{d}}{\mathrm{d}\phi} P_n(\sin\phi) - \frac{1}{\cos\phi}\frac{\mathrm{d}}{\mathrm{d}\phi} P_{n+1}(\sin\phi) = 0. \end{gathered} \tag{9}$$

The gradient line in question then follows (Köhnlein, 1966)

$$\sin\phi + \sum_{n=2}^{\infty} \left(\frac{a}{r}\right)^n \frac{n+1}{n} J_n\left[\sin\phi\, P_n(\sin\phi) - P_{n+1}(\sin\phi)\right] + C = 0, \tag{10}$$

with an integration constant $C$ depending on the point $r_0$, $\phi_0$ through which the trajectory runs (initial value problem). The summation term in (10) becomes zero for $r$ going to infinity; hence,

$$\lim_{r\to\infty} \phi = \bar{\phi} = \arcsin(-C), \tag{11}$$

which means that the trajectory through $r_0$, $\phi_0$ has the selenographic latitude $\bar{\phi}$ as asymptote.

## 2. Shape of the Gradient Line

Table I gives the distance

$$d = r\sin(\bar{\phi} - \phi) \tag{12}$$

TABLE I

Distance of the trajectory from its asymptote (in meters)

| $\phi°$ | | d [m] $h=0$ (km) | $h=10$ (km) | $h=100$ (km) | $h=250$ (km) | $h=500$ (km) | $h=1000$ (km) | $h=5000$ (km) | $h=10000$ (km) | $h=50000$ (km) | Asymptotic latitude $\bar{\phi}°$ |
|---|---|---|---|---|---|---|---|---|---|---|---|
| 90 | L | 0 | 0 | 0 | 0 | 0 | 0 | 0 | 0 | 0 | 90 |
| | M | 0 | 0 | 0 | 0 | 0 | 0 | 0 | 0 | 0 | 90 |
| 80 | L | 118.5 | 115.4 | 95.4 | 79.2 | 67.5 | 55.5 | 23.0 | 13.2 | 3.0 | 80.0039 |
| | M | 82.5 | 81.6 | 76.0 | 71.4 | 66.2 | 56.6 | 23.8 | 13.7 | 3.1 | 80.0027 |
| 70 | L | 127.5 | 128.8 | 135.4 | 134.9 | 125.3 | 105.0 | 43.3 | 24.9 | 5.6 | 70.0042 |
| | M | 136.3 | 137.2 | 141.1 | 139.0 | 128.6 | 107.8 | 44.8 | 25.8 | 5.8 | 70.0045 |
| 60 | L | 231.5 | 229.5 | 214.5 | 196.4 | 174.3 | 143.1 | 58.4 | 33.5 | 7.6 | 60.0076 |
| | M | 250.3 | 247.8 | 228.5 | 205.8 | 180.3 | 147.3 | 60.5 | 34.7 | 7.9 | 60.0083 |
| 50 | L | 263.3 | 261.8 | 248.3 | 228.4 | 201.7 | 164.1 | 76.4 | 38.1 | 8.6 | 50.0087 |
| | M | 265.8 | 264.0 | 250.1 | 231.1 | 205.8 | 168.9 | 68.8 | 39.5 | 8.9 | 50.0088 |
| 40 | L | 261.4 | 259.9 | 247.5 | 228.6 | 202.3 | 164.6 | 66.4 | 38.0 | 8.6 | 40.0086 |
| | M | 241.2 | 241.5 | 240.0 | 229.5 | 207.5 | 170.3 | 68.9 | 39.5 | 8.9 | 40.0080 |
| 30 | L | 233.9 | 232.2 | 218.3 | 200.2 | 177.1 | 144.5 | 58.3 | 33.4 | 7.6 | 30.0077 |
| | M | 274.8 | 271.4 | 246.3 | 218.1 | 188.1 | 151.2 | 60.6 | 34.7 | 7.9 | 30.0091 |
| 20 | L | 156.2 | 156.0 | 152.7 | 144.4 | 130.1 | 106.9 | 43.2 | 24.8 | 5.6 | 20.0052 |
| | M | 176.7 | 175.8 | 167.8 | 155.5 | 137.9 | 112.2 | 44.9 | 25.7 | 5.8 | 20.0058 |
| 10 | L | 94.8 | 94.0 | 87.6 | 79.7 | 70.0 | 56.6 | 22.8 | 13.1 | 3.0 | 10.0031 |
| | M | 66.1 | 67.1 | 73.2 | 75.3 | 71.0 | 59.2 | 23.7 | 13.6 | 3.1 | 10.0022 |
| 0 | L | 8.1 | 7.8 | 5.6 | 2.8 | 0.4 | −0.9 | −0.32 | −0.110 | −0.006 | 0.0003 |
| | M | 25.3 | 23.9 | 14.4 | 6.5 | 1.7 | −0.6 | −0.34 | −0.116 | −0.006 | 0.0008 |
| −10 | L | −91.0 | −90.7 | −87.8 | −82.0 | −72.9 | −59.2 | −23.3 | −13.3 | −3.0 | −10.0030 |
| | M | −85.8 | −85.5 | −83.2 | −80.0 | −73.8 | −61.5 | −24.3 | −13.8 | −3.1 | −10.0028 |
| −20 | L | −192.7 | −190.8 | −176.2 | −158.5 | −137.5 | −110.0 | −43.4 | −24.8 | −5.6 | −20.0064 |
| | M | −195.1 | −194.0 | −183.9 | 167.8 | −145.8 | −115.8 | −45.2 | −25.8 | −5.8 | −20.0064 |
| −30 | L | −232.8 | −231.9 | −222.3 | −205.3 | −180.6 | −145.5 | −58.2 | −33.4 | −7.6 | −30.0077 |
| | M | −289.3 | −286.1 | −261.1 | −229.9 | −194.8 | −153.3 | −60.5 | −34.6 | −7.9 | −30.0095 |
| −40 | L | −268.8 | −266.3 | −247.3 | −224.6 | −197.8 | −161.4 | −65.8 | −37.9 | −8.6 | −40.0089 |
| | M | −273.9 | −271.4 | −252.6 | −230.5 | −204.3 | −167.4 | −68.3 | −39.3 | −8.9 | −40.0090 |

*Table I (Continued)*

| | | | | | | | | | | | |
|---|---|---|---|---|---|---|---|---|---|---|---|
| −50 | L | −215.7 | −215.6 | −213.2 | −204.9 | −187.9 | −157.3 | −65.5 | −37.8 | −8.6 | −50.0071 |
| | M | −159.9 | −163.2 | −182.9 | −193.0 | −187.0 | −160.9 | −67.9 | −39.2 | −8.9 | −50.0053 |
| −60 | L | −190.6 | −190.6 | −188.2 | −179.4 | −163.1 | −136.3 | −57.4 | −33.2 | −7.6 | −60.0063 |
| | M | −244.7 | −241.4 | −217.8 | −192.9 | −168.6 | −139.5 | −59.4 | −34.4 | −7.8 | −60.0081 |
| −70 | L | −207.2 | −202.7 | −172.7 | −145.8 | −123.7 | −100.7 | −42.5 | −24.6 | −5.6 | −70.0068 |
| | M | −213.3 | −209.1 | −179.6 | −151.3 | −127.2 | −103.0 | −43.9 | −25.5 | −5.8 | −70.0070 |
| −80 | L | −6.2 | −11.2 | −41.1 | −59.1 | −61.8 | −53.2 | −22.6 | −13.1 | −3.0 | −80.0002 |
| | M | 55.4 | 47.2 | −5.3 | −43.1 | −57.8 | −53.6 | −23.3 | −13.6 | −3.2 | −79.9982 |
| −90 | L | 0 | 0 | 0 | 0 | 0 | 0 | 0 | 0 | 0 | −90 |
| | M | 0 | 0 | 0 | 0 | 0 | 0 | 0 | 0 | 0 | −90 |

L = by use of Liu's coefficients.
M = by use of Michael's coefficients.

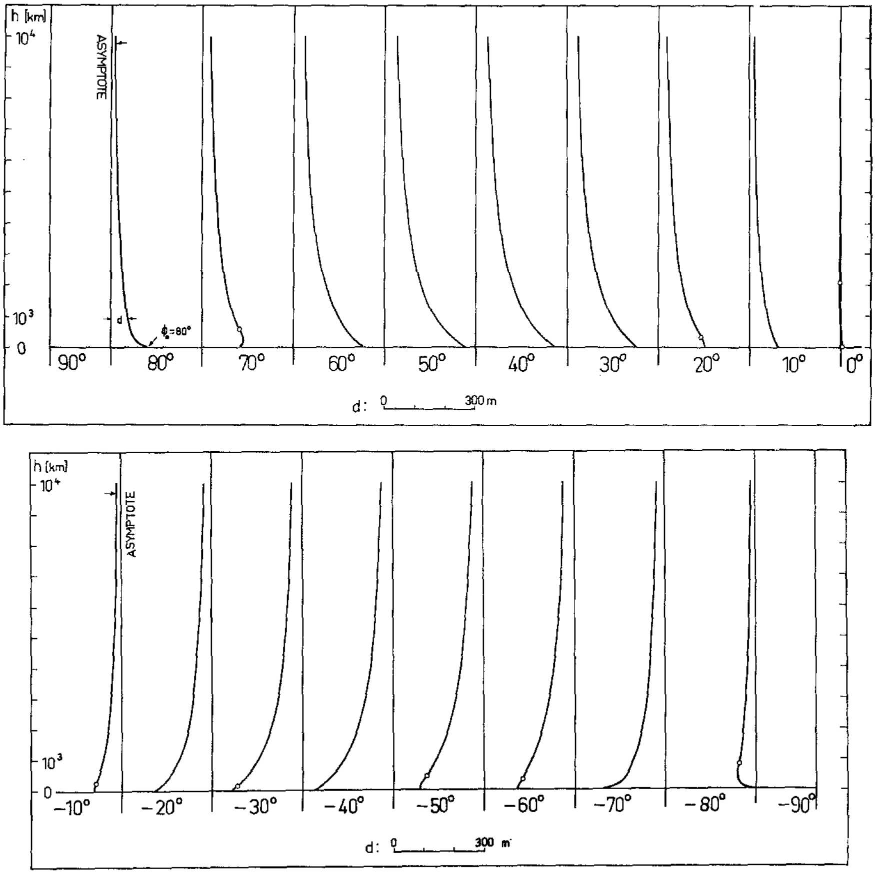


Fig. 1. Shape of the gradient line along a meridian $r_0 = a$, $\phi_0 = 90°, 80°, \ldots, -90°$ (Liu's coefficients). The circles indicate points of inflection.

of a point $r$, $\phi$ on the trajectory from its asymptote $\bar{\phi}$ for both the Liu* and Michael coefficients. The initial points $r_0$, $\phi_0$ were taken along a circle with the radius $r_0 = a$, with $\phi_0$ varying in tens of degrees from 90° to −90°. The sign of $d$ is assumed to be positive for a point $r$, $\phi$ south of the asymptote $\bar{\phi}$, otherwise it is negative. Figure 1 shows a picture of the trajectories relative to their asymptotes. The scale for the distance $d$ was taken 10000 times dilated compared to the elevation $h$ (above $r_0 = a$), and hence the shape of the gradient line is highly overemphasized. For example, the tangent in $r_0 = a$, $\phi_0 = 40°$ and the corresponding asymptote $\bar{\phi}_{40}$** seem to include in Figure 1 an angle of about 45°; however, both lines intersect actually with an angle of 29″ as shown in Table III.

In the northern hemisphere the gradient line approaches – in general – the asymptote from the south while the opposite is true for the southern hemisphere. The distance

* All numerical results refer to the coefficients of Liu and Laing, if not otherwise stated. For brevity, we write only Liu and analogously Michael for Michael *et al.* (1969).

** $\bar{\phi}_{40}$ means $\bar{\phi}$ of $r_0 = a$, $\phi_0 = 40°$.

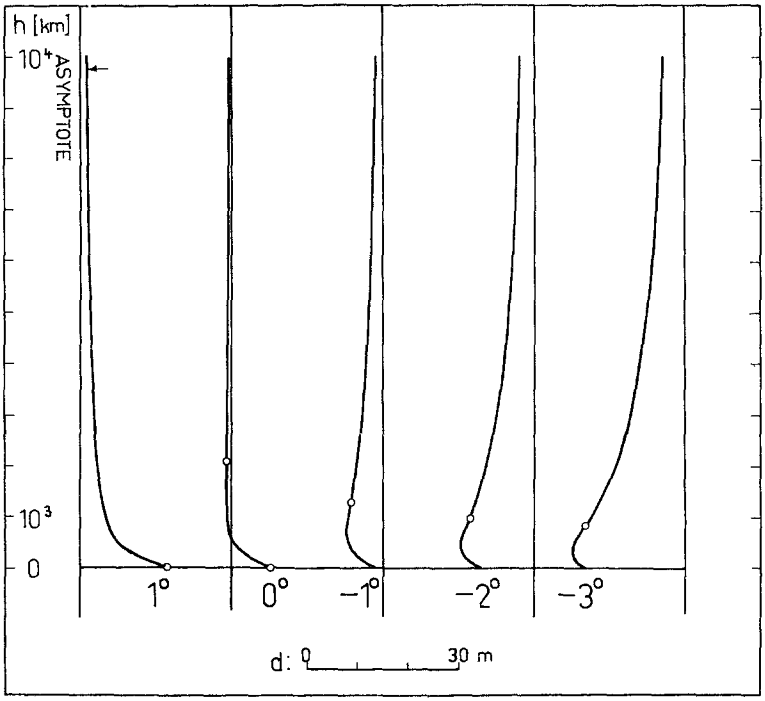


Fig. 2. Shape of the gradient line around the selenographic equator $r_0 = a$, $\phi_0 = 1°, 0°, \ldots$ (Liu's coefficients).

$d$ is zero at the poles and increases in magnitude towards middle latitudes: for Liu's coefficients $d$ becomes 263 m at $r_0 = a$, $\phi_0 = 50°$, and 269 m at $r_0 = a$, $\phi_0 = -40°$. At higher elevations, such as 10000 km above $r_0 = a$, the corresponding values decrease rapidly to about 8.6 m. As seen from Table I and Figure 1 most of the change in $d$ takes place within the first 1000 km elevation. From then on, the gradient line approaches asymptotically its corresponding radius vector $\bar{\phi} = \text{const}$. If we plot the distance $d$ against the latitude $\phi$ (for the same elevation), we get a sinusoidal curve with zeros at the poles, extrema in middle latitudes and almost zero at the equator $\phi = 0°$.

In fact, the equatorial region needs particular consideration. Figure 2 shows the transitional stage between $1° > \phi > -3°$. To get a detailed picture, the $d$-scale was dilated against the $h$-scale by a factor of 100000. Due to the odd zonal coefficients $J_{2n-1}$ there is no symmetry between the northern and the southern part. In fact, the typical northern structure tends to impress its pattern down to about $\phi_0 \sim -3°$; only from thereon the trajectory assumes its characteristic southern shaped structure. Noteworthy is also the reversal of directional approach of the gradient line towards its asymptote (Figure 2).

Another exceptional pattern is seen on the southern hemisphere within the selenographic latitudes $-75° > \phi > -90°$. Up to about 500 km elevation, the southern-shape structure of the trajectory is completely reversed (Figure 3) due to the strong influence

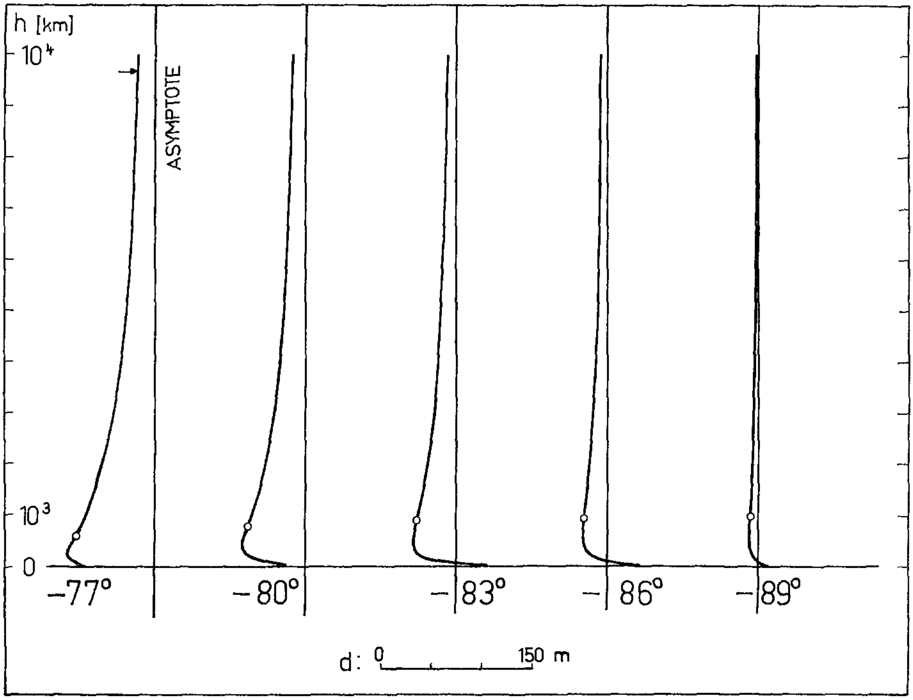


Fig. 3. Shape of the gradient line near the south pole $r_0 = a$, $\phi_0 = -77°, -80°, \ldots$ (Liu's coefficients).

of the odd zonal coefficients of higher degrees. For example, in the latitude $-85°$ the initial point $r_0$, $\phi_0$ lies 36.9 m south of $\bar{\phi}_{-85}$.

In order to find the points $r_0$, $\phi_0$ which coincide with their asymptotes, we make use of the expression

$$\sum_{n=2}^{\infty} \left(\frac{a}{r}\right)^n \frac{1}{n} J_n \frac{\mathrm{d}}{\mathrm{d}\phi} P_n(\sin\phi) = 0 \tag{13}$$

by putting $\phi_0 = \bar{\phi}$ in (10). Solving this equation numerically, we find for Liu's coefficients two real roots (the roots at the poles are trivial), namely at $r_0 = a$,

$$\phi_0 \sim -80\overset{\circ}{.}365$$

and

$$\phi_0 \sim -\ 0\overset{\circ}{.}872.$$

The last root lies in the transition zone shown by Figure 2 about 26.6 km south of the selenographic equator.

An insight into the straightness of the gradient line can be obtained by comparing its length up to infinity with the corresponding radii vectors. Starting from the arc length $s_{12}$ between the two curve points $r_1$, $\phi_1$ and $r_2$, $\phi_2$

TABLE II

Angle of intersection between tangent and radius vector

| $\phi°$ | $\nu$ $h = 0$ km L | M | $h = 250$ km L | M | $h = 1000$ km L | M | $h = 10000$ km L | M |
|---|---|---|---|---|---|---|---|---|
| 90 | 0″ | 0″ | 0″ | 0″ | 0″ | 0″ | 0″ | 0″ |
| 80 | 1′21″ | 29″ | 22″.9 | 12″.2 | 8″.1 | 7″.9 | 0″.465 | 0″.482 |
| 70 | − 14″ | − 3″ | 19″.4 | 21″.0 | 15″.3 | 15″.6 | 0″.874 | 0″.906 |
| 60 | 1′10″ | 1′23″ | 41″.7 | 47″.4 | 21″.4 | 22″.0 | 1″.178 | 1″.221 |
| 50 | 1′ 3″ | 1′ 8″ | 48″.8 | 47″.6 | 24″.9 | 25″.3 | 1″.339 | 1″.389 |
| 40 | 1′ 0″ | 22″ | 48″.0 | 41″.2 | 25″.0 | 25″.7 | 1″.338 | 1″.389 |
| 30 | 1′ 5″ | 1′44″ | 42″.8 | 54″.1 | 21″.9 | 23″.3 | 1″.175 | 1″.220 |
| 20 | 23″ | 39″ | 27″.0 | 32″.2 | 16″.1 | 17″.1 | 0″.870 | 0″.904 |
| 10 | 29″ | − 15″ | 17″.7 | 8″.8 | 8″.7 | 8″.9 | 0″.460 | 0″.478 |
| 0 | 6″ | 34″ | 3″.3 | 7″.6 | 0″.08 | 0″.26 | −0″.0058 | −0″.0061 |
| −10 | − 16″ | − 17″ | −16″.6 | −13″.0 | −9″.1 | −9″.2 | −0″.469 | −0″.488 |
| −20 | −1′ 3″ | − 46″ | −37″.3 | −38″.1 | −17″.2 | −18″.4 | −0″.875 | −0″.909 |
| −30 | − 47″ | −1′40″ | −43″.9 | −60″.1 | −22″.5 | −24″.4 | −1″.173 | −1″.218 |
| −40 | −1′24″ | −1′26″ | −49″.9 | −49″.7 | −24″.3 | −25″.1 | −1″.329 | −1″.379 |
| −50 | − 27″ | 52″ | −34″.5 | −17″.2 | −22″.8 | −22″.6 | −1″.324 | −1″.373 |
| −60 | − 21″ | −1′38″ | −32″.1 | −46″.6 | −19″.7 | −20″.1 | −1″.161 | −1″.203 |
| −70 | −2′ 0″ | −1′56″ | −41″.3 | −44″.0 | −14″.8 | −15″.2 | −0″.860 | −0″.890 |
| −80 | −1′47″ | 3′ 3″ | 4″.7 | 24″.1 | − 7″.6 | − 7″.2 | −0″.457 | −0″.473 |
| −90 | 0″ | 0″ | 0″ | 0″ | 0″ | 0″ | 0″ | 0″ |

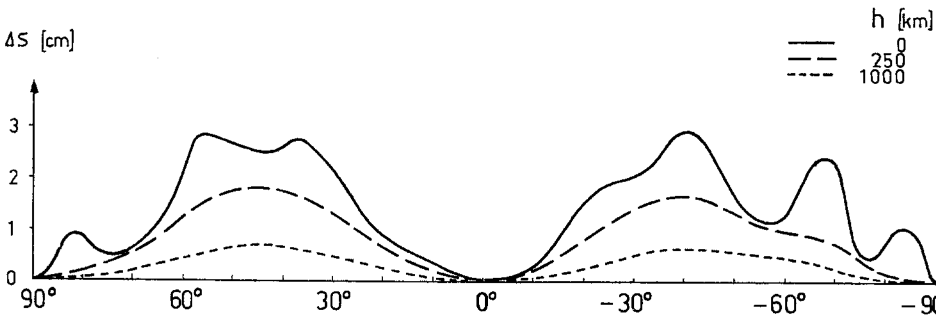


Fig. 4. Difference between the total length of the gradient line and its corresponding radii vectors (Liu's coefficients).

$$s_{12} = \int_{r_1}^{r_2} \sqrt{1 + \left(r \frac{\mathrm{d}\phi}{\mathrm{d}r}\right)^2} \, \mathrm{d}r, \tag{14}$$

we obtain the difference towards the corresponding radii for $r_2 \to \infty$

$$\Delta s = \int_{r_1}^{\infty} \left[\sqrt{1 + \left(r \frac{\mathrm{d}\phi}{\mathrm{d}r}\right)^2} - 1\right] \mathrm{d}r. \tag{15}$$

Figure 4 shows the numerical results for Liu's coefficients with

$r_1 = a$

$r_1 = a + 250$ km

$r_1 = a + 1000$ km

and $r_2 \to \infty$. The greatest deviation of $\Delta s$ is about 3 cm for $r_1 = a$ and $\phi \sim -40°$. Again we have a sinusoidal pattern: $\Delta s$ equals to zero at the poles, with maxima in middle latitudes and fractions of a millimeter (for $r_1 = a$) in the neighbourhood of the equator. At $h = 250$ km the $\Delta s$ variation is already very smooth and the shape of the trajectory is closely resembled by a hyperbola.

## 3. Direction and Curvature

The direction of the tangent in each point of the trajectory is given by Equation (3). Intersecting it with the corresponding radius vector, the angle

$$v = \arcsin \frac{1}{r\,|\mathrm{grad}\, U|} \frac{\partial U}{\partial \phi} \tag{16}$$

represents the directional field of the differential Equation (3) in a spherical coordinate system. The different elevations $h$ in Table II refer to the same selenographic latitude and hence the values do not lie on the same gradient line. As shown in Figure 5 the pattern is unchanged from the previous ones: zeros at the poles, extrema – in general – in middle latitudes and almost zero around the equator. The angle $v$ is positively

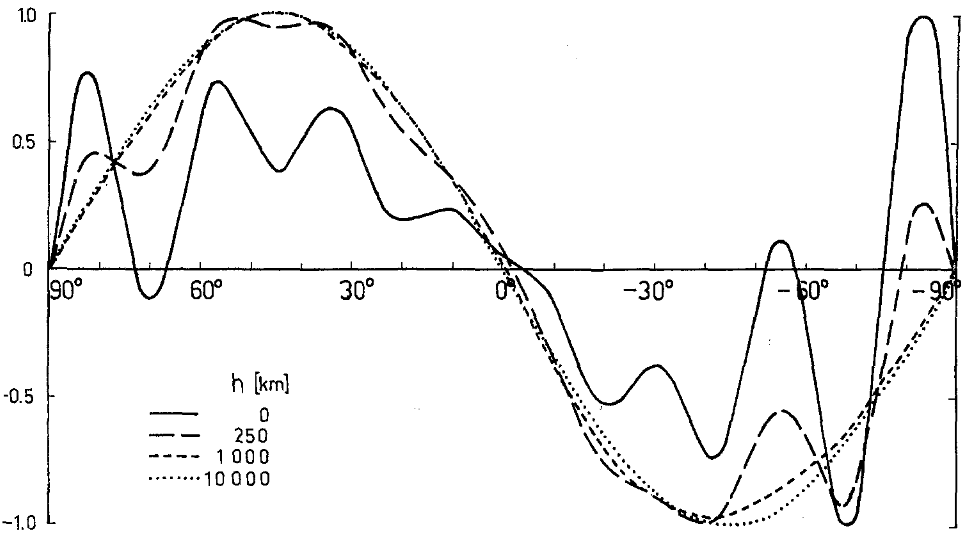


Fig. 5. Angle (normalized) of intersection between the tangent of the gradient line and the corresponding radius vector (Liu's coeff.) Angle (actual, in seconds of arc): the normalized angles must be multiplied by 120″.0 ($h = 0$ km); 50″.0 ($h = 250$ km); 25″.4 ($h = 1000$ km); 1″.4 ($h = 10000$ km).

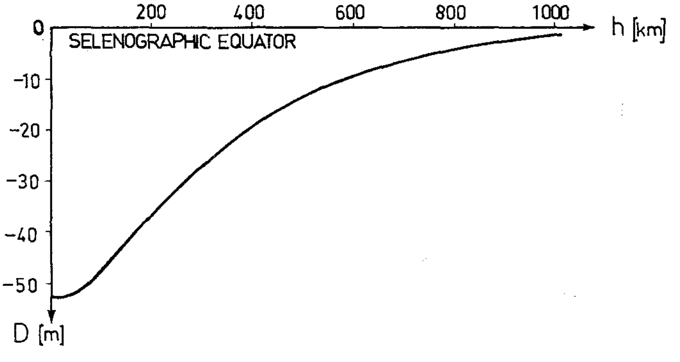


Fig. 6. Actual equator: loci of all points in which the tangent of a gradient line is parallel to the selenographic equator (Liu's coefficients).

counted if the trajectory intersects the corresponding radius vector under an angle of slope greater than $\phi$. In the southern hemisphere $\nu$ reaches the extremum $-2'$ in $r_0 = a$, $\phi_0 = -70°$ which reduces at higher elevations to $-1''.3$ at $h = 10000$ km and $\phi = -45°$.

Figure 6 gives the curve loci of all points of the actual zonal equator. Herein $\nu$ equals $-\phi$. At zero elevation the actual equator lies approximately 53 m south of the selenographic equator. This distance $D$ rapidly decreases to about 1 m at 1000 km elevation, for example.

If we consider the angle of intersection between the tangent of a gradient line and its asymptote

TABLE III

Angle of intersection between tangent and asymptote

| $\phi°$ | $\gamma$ (seconds of arc) | | | | | | | |
|---|---|---|---|---|---|---|---|---|
| | $h=0$ km | | $h=250$ km | | $h=1000$ km | | $h=10000$ km | |
| | L | M | L | M | L | M | L | M |
| 90 | 0 | 0 | 0 | 0 | 0 | 0 | 0 | 0 |
| 80 | 67 | 20 | 15 | 5 | 3.9 | 3.6 | 0.233 | 0.241 |
| 70 | −29 | −19 | 5 | 7 | 7.4 | 7.5 | 0.438 | 0.453 |
| 60 | 42 | 53 | 21 | 26 | 10.6 | 10.9 | 0.590 | 0.611 |
| 50 | 32 | 36 | 25 | 24 | 12.5 | 12.6 | 0.670 | 0.695 |
| 40 | 29 | − 7 | 24 | 17 | 12.6 | 12.8 | 0.670 | 0.695 |
| 30 | 37 | 72 | 22 | 31 | 11.0 | 11.9 | 0.588 | 0.611 |
| 20 | 4 | 18 | 12 | 16 | 8.0 | 8.7 | 0.435 | 0.452 |
| 10 | 18 | −23 | 9 | 1 | 4.4 | 4.4 | 0.229 | 0.239 |
| 0 | 5 | 31 | 3 | 7 | 0.15 | 0.31 | −0.0038 | 0.0040 |
| −10 | − 5 | − 7 | −8 | − 5 | − 4.6 | − 4.6 | −0.236 | −0.245 |
| −20 | −40 | −23 | −21 | −21 | − 8.9 | − 9.7 | −0.438 | −0.456 |
| −30 | −19 | −66 | −23 | −36 | −11.5 | −12.9 | −0.587 | −0.610 |
| −40 | −53 | −53 | −27 | −26 | −12.1 | −12.5 | −0.664 | −0.689 |
| −50 | − 1 | 71 | −13 | 3 | −11.0 | −10.5 | −0.661 | −0.684 |
| −60 | 1 | −69 | −13 | −27 | − 9.4 | − 9.6 | −0.579 | −0.599 |
| −70 | −95 | −90 | −26 | −28 | − 7.3 | − 7.4 | −0.428 | −0.442 |
| −80 | 107 | 176 | −11 | 28 | − 3.6 | − 3.1 | −0.227 | −0.234 |
| −90 | 0 | 0 | 0 | 0 | 0 | 0 | 0 | 0 |

TABLE IV

Radius of curvature

| $\phi°$ | $\varrho$ (in km) $h=0$ km | | $h=250$ km | | $h=1000$ km | | $h=10000$ km | |
|---|---|---|---|---|---|---|---|---|
| | L | M | L | M | L | M | L | M |
| 90 | ∞ | ∞ | ∞ | ∞ | ∞ | ∞ | ∞ | ∞ |
| 80 | 416E3 | 120E4 | 310E4 | 203E5 | 764E5 | 134E6 | 520E7 | 504E7 |
| 70 | 602E3 | 831E3 | 531E4 | 677E4 | 482E5 | 469E5 | 276E7 | 268E7 |
| 60 | 111E4 | 995E3 | 595E4 | 381E4 | 276E5 | 252E5 | 205E7 | 198E7 |
| 50 | 133E5 | 215E4 | 738E4 | 753E4 | 216E5 | 232E5 | 180E7 | 174E7 |
| 40 | 223E5 | 844E3 | 905E4 | 985E4 | 216E5 | 230E5 | 180E7 | 174E7 |
| 30 | 182E4 | 652E3 | 667E4 | 277E4 | 257E5 | 212E5 | 205E7 | 197E7 |
| 20 | 229E4 | 140E6 | 611E5 | 155E5 | 374E5 | 321E5 | 278E7 | 267E7 |
| 10 | 289E4 | 999E3 | 140E5 | 594E4 | 595E5 | 803E5 | 529E7 | 507E7 |
| 0 | 624E5 | 994E3 | 200E5 | 567E4 | 270E6 | 176E6 | 216E9 | 207E9 |
| −10 | 409E4 | 256E4 | 720E5 | 522E5 | 606E5 | 843E5 | 508E7 | 487E7 |
| −20 | 134E4 | 904E4 | 552E4 | 101E5 | 278E5 | 247E5 | 275E7 | 264E7 |
| −30 | 237E4 | 117E4 | 133E5 | 234E4 | 221E5 | 171E5 | 206E7 | 198E7 |
| −40 | 995E3 | 854E3 | 425E4 | 454E4 | 229E5 | 233E5 | 183E7 | 176E7 |
| −50 | 197E4 | 358E3 | 134E5 | 202E4 | 317E5 | 496E5 | 184E7 | 178E7 |
| −60 | 121E4 | 606E3 | 280E5 | 273E4 | 349E5 | 304E5 | 211E7 | 205E7 |
| −70 | 329E3 | 398E3 | 207E4 | 203E4 | 352E5 | 318E5 | 286E7 | 278E7 |
| −80 | 224E3 | 159E3 | 173E4 | 964E3 | 120E6 | 607E6 | 539E7 | 524E7 |
| −90 | ∞ | ∞ | ∞ | ∞ | ∞ | ∞ | ∞ | ∞ |

E3 means $10^3$.

$$\gamma = \operatorname{arctg}\left(\frac{\operatorname{tg}\beta - \operatorname{tg}\bar{\phi}}{1 + \operatorname{tg}\beta \operatorname{tg}\bar{\phi}}\right) \tag{17}$$

with

$$\beta = \phi + \operatorname{arctg}\left(r\Big/\frac{\mathrm{d}r}{\mathrm{d}\phi}\right), \tag{18}$$

we get the values $\gamma$ for the different elevations along the same trajectory as shown in Table III. The sign of $\gamma$ is analogously defined as that for $\nu$. In $\phi = -80°$ the angle $\gamma$ amounts to 107″, i.e. the maximum at zero elevation. At 10000 km elevation the angle of intersection reaches its extremum $|\gamma| = 0\overset{''}{.}670$ in the latitude $|\phi| \sim 45°$.

The change of $\gamma$ along the same trajectory leads to the radius of curvature

$$\varrho = \frac{1}{\sqrt{\dfrac{\mathrm{d}^2\mathbf{x}}{\mathrm{d}s^2}\dfrac{\mathrm{d}^2\mathbf{x}}{\mathrm{d}s^2}}}, \tag{19}$$

which is infinite at the poles, decreases in general towards middle latitudes and reaches again large values near the equator. This can be seen at least for higher elevations ($\sim$1000 km) in Table IV, while for lower elevations the disturbance of high degree coefficients is clearly visible.

Along the same gradient line the radius of curvature increases in general with higher elevation. The only exceptions are those trajectories which have points of inflections:

$$r^2 + 2\left(\frac{\mathrm{d}r}{\mathrm{d}\phi}\right)^2 - r\frac{\mathrm{d}^2 r}{\mathrm{d}\phi^2} = 0, \tag{20}$$

such as in Figures 2, 3 and partly in Figure 1 (marked by circles). Here, the radius of curvature becomes infinite and the shape of the trajectory changes its pattern.

## 4. Conclusions

The Moon's gradient line shows a stronger structural variety than the corresponding trajectory of the Earth's field (Köhnlein, 1966). Most of the variation of the geometric shape takes place within the first 1000 km above the Moon's surface. From then on, the gradient line behaves like a hyperbola approaching its asymptote very quickly with higher elevation.

At the poles the gradient line is a straight line and coincides with its selenographic radius vector. Toward middle latitudes the trajectory is, in general, bent to the south on the northern hemisphere, and vice versa on the southern hemisphere. With decreasing selenographic latitude ($|\phi| \to 0°$) the gradient line becomes rather straight and changes its asymptotical approach at the equator. Near the south pole the general pattern is completely disturbed due to an accumulating effect of the higher degree harmonics. The gradient line is bent to the south and only changes its pattern at higher elevation (points of inflection).

Along a meridian the variation of the direction field, the straightness of the trajectory, etc., are, in general, sinusoidal (at least at higher elevations): zero deviations at the poles, small ones at the equator and extrema in middle latitudes, while for the radius of curvature – for geometrical reasons – the opposite is true.

The numerical results derived from Liu's and Michael's coefficients differ indeed in details but show a rather good agreement in the overall structure of the Moon's gradient line. By taking instead the coefficients of Blackshear *et al.* (1971), the resulting gradient line deviates somewhat stronger from both the Liu and the Michael values.

## Acknowledgments

This work was supported by grant WRK 226 from the Bundesministerium für Bildung und Wissenschaft.

## Constants and Coefficients Used

$a = 1\,738\,090$ m, mean equatorial radius of the Moon
$GM = 4.90278 \times 10^{12}$ m$^3$ s$^{-2}$, gravitational constant × mass of the Moon

Harmonic coefficients

| | Liu | Michael |
|---|---|---|
| $J_2$ | $0.1996 \times 10^{-3}$ | $0.20707 \times 10^{-3}$ |
| $J_3$ | $0.5878 \times 10^{-5}$ | $0.6303 \times 10^{-5}$ |
| $J_4$ | $-0.1195 \times 10^{-4}$ | $-0.1938 \times 10^{-4}$ |
| $J_5$ | $0.4544 \times 10^{-5}$ | $0.7459 \times 10^{-5}$ |
| $J_6$ | $-0.1088 \times 10^{-5}$ | $0.1078 \times 10^{-5}$ |
| $J_7$ | $-0.1779 \times 10^{-4}$ | $-0.2408 \times 10^{-4}$ |
| $J_8$ | $0.5967 \times 10^{-5}$ | $0.2655 \times 10^{-4}$ |
| $J_9$ | $0.3206 \times 10^{-5}$ | $0.1543 \times 10^{-5}$ |
| $J_{10}$ | $-0.1367 \times 10^{-5}$ | $-0.5634 \times 10^{-4}$ |
| $J_{11}$ | $0.7311 \times 10^{-5}$ | $0.2460 \times 10^{-4}$ |
| $J_{12}$ | $-0.1251 \times 10^{-4}$ | $-0.3299 \times 10^{-4}$ |
| $J_{13}$ | $0.3315 \times 10^{-4}$ | $0.5772 \times 10^{-4}$ |
| $J_{14}$ | $-0.1044 \times 10^{-4}$ | |
| $J_{15}$ | $0.2977 \times 10^{-4}$ | |

## References

Blackshear, W. T., Daniels, E. F., and Anderson, S. G.: 1971, NASA-TM-X-2260.
Hobson, E. W.: 1955, *The Theory of Spherical and Ellipsoidal Harmonics*, Chelsea Publishing Co., New York.
Köhnlein, W.: 1966, Smithsonian Astrophys. Obs. Spec. Rep. No. 216.
Liu, A. S. and Laing, P. A.: 1971, *Science* **173**, 1017–1020.
Michael, W. H., Jr., Blackshear, W. T., and Gapcynski, J. P.: 1969, Plenary meeting COSPAR, 12th, Prague.